Preprints of the 21st IFAC World Congress (Virtual)
Berlin, Germany, July 12-17, 2020

A predictive path-following controller for multi-steered articulated vehicles ⋆

Oskar Ljungqvist * **Daniel Axehill** *

* *Division of Automatic Control, Linköping University, 581 83 Linköping, Sweden (e-mail: oskar.ljungqvist@liu.se, daniel.axehill@liu.se).*

Abstract: Stabilizing multi-steered articulated vehicles in backward motion is a complex task for any human driver. Unless the vehicle is accurately steered, its structurally unstable joint-angle kinematics during reverse maneuvers can cause the vehicle segments to fold and enter a jack-knife state. In this work, a model predictive path-following controller is proposed enabling automatic low-speed steering control of multi-steered articulated vehicles, comprising a car-like tractor and an arbitrary number of trailers with passive or active steering. The proposed path-following controller is tailored to follow nominal paths that contains full state and control-input information, and is designed to satisfy various physical constraints on the vehicle states as well as saturations and rate limitations on the tractor's curvature and the trailer steering angles. The performance of the proposed model predictive path-following controller is evaluated in a set of simulations for a multi-steered 2-trailer with a car-like tractor where the last trailer has steerable wheels.

Keywords: Path-following control, multi-steered N-trailers, tractor-trailer vehicles

1. INTRODUCTION

The transportation sector faces growing demands from the society to increase efficiency and to reduce the environmental footprint related to freight and public transport. As a result, recent trends in modern transport include an increased interest in large capacity (multi-) articulated buses (Michalek, 2019) and long tractor-trailer combinations (Islam et al., 2015). In order to improve these long vehicle's maneuvering capability, some of the trailers are equipped with steerable wheels. Compared to single-steered N-trailer (SSNT) vehicles where all trailers are passive, multi-steered N-trailer (MSNT) vehicles are more agile, but also significantly more difficult to control for a human driver. This is partly because of the vehicle's additional degrees of freedom and partly due to specific kinematic and dynamics properties of MSNT vehicles (Tilbury et al., 1995; Islam et al., 2015; Orosco-Guerrero et al., 2002; Michalek, 2019). To aid the driver, various control systems have been proposed to automatically control the steerable trailer wheels to either decrease the turning radius during reverse maneuvers or to diminish the so-called off-tracking effect during tight cornering (Beyersdorfer and Wagner, 2013; Odhams et al., 2011; Varga et al., 2018; Van De Wouw et al., 2015; Michalek, 2019).

Even though several feedback-control strategies have been proposed for various SSNT vehicles (see e.g. Michalek (2014); Ljungqvist et al. (2019); Altafini et al. (2001); Rimmer and Cebon (2017); Altafini (2003)), only a limited amount of work has been devoted to the path-following or the trajectory-tracking control problem for special classes of MSNT vehicles (see e.g. Odhams et al. (2011); Varga et al. (2018); Van De Wouw et al. (2015); Yuan et al. (2015); Sadeghi et al. (2019)). However, these approaches mainly use the additional trailer-steering capability to reduce the off-tracking effect while tracking a geometric reference path or trajectory. As a consequence, there is still a need to present a path-following controller for a generic MSNT vehicle for the case when the nominal path contains full state and control-input information, i.e., it is tailored to operate in series with a motion planner similar to Evestedt et al. (2016); Li et al. (2019); Beyersdorfer and Wagner (2013); Ljungqvist et al. (2019); Bergman et al. (2020).

The contribution of this work is a path-following controller for a generic MSNT with a car-like tractor targeting low-speed maneuvers, which is designed to operate in series with a motion planner that computes feasible paths. It is done by first deriving a path-following error model describing the vehicle in terms of deviation from the nominal path. This error model together with physical constraints on states and control inputs are then used to design a path-following controller based on the framework of model predictive control (MPC) (Mayne et al., 2000; Garcia et al., 1989; Faulwasser et al., 2015; Lima et al., 2017). To the best of the authors' knowledge, this paper presents the first path-following controller for a generic MSNT with a car-like tractor admitting mixtures of off-axle/on-axle hitch connections and steerable/non-steerable trailers, and is designed to satisfy various constraints on states and control inputs.

The remainder of the paper is structured as follows. The kinematic vehicle model is presented in Section 2 and the path-following error model is derived in Section 3. The proposed model predictive path-following controller is presented in Section 4. In Section 5, simulation results for a MS2T with a car-like tractor is presented and the paper is concluded in Section 6 by summarizing the contributions and discussing directions for future work.

⋆ This work was funded by FFI/VINNOVA.

2. KINEMATIC VEHICLE MODEL

The MSNT with a car-like tractor considered in this work is composed of $N+1$ interconnected vehicle segments, including a leading car-like tractor and N number of trailers that are either passively of actively steered. The car-like tractor has a steerable front wheel and its rear wheel is fixed. The MSNT vehicle is illustrated in Fig. 1, where each vehicle segment is described by a segment length $L_i > 0$ and a signed hitching offset M_i. Since low-speed maneuvers are considered, a kinematic model is used to describe the vehicle. The model is based on the work in Michalek (2019) and is derived based on some assumptions including that the wheels are rolling without slipping. By considering the steering angles as control inputs, the MSNT with a car-like tractor can be described with a state vector that consists of $n = 3 + N$ variables:

- the global pose (x_N, y_N, θ_N) of the Nth trailer in a fixed coordinate frame
$$q_N = [x_N \ y_N \ \theta_N]^\mathsf{T} \in \mathbb{R}^2 \times \mathbb{S}, \tag{1}$$
where $\mathbb{S} = (-\pi, \pi]$.
- for $i = 1, \ldots, N$, a number of N constrained joint angles
$$\beta_i = \theta_{i-1} - \theta_i \in \mathcal{B}_i = [-\bar{\beta}_i, \bar{\beta}_i], \quad \bar{\beta}_i \in (0, \pi/2). \tag{2}$$
The state vector for the MSNT with a car-like tractor is defined as
$$x = \left[q_N^\mathsf{T} \ \beta_N \ \beta_{N-1} \ \ldots \ \beta_1\right]^\mathsf{T} \in \mathcal{X}, \tag{3}$$
where $\mathcal{X} = \mathbb{R}^2 \times \mathbb{S} \times \mathcal{B}_N \times \mathcal{B}_{N-1} \times \ldots \times \mathcal{B}_1$.

By treating the longitudinal velocity of the car-like tractor v_0 as an exogenous input, the control input consists of $m = 1 + S$ variables:

- the curvature of the car-like tractor $\kappa_0 = \frac{\tan\beta_0}{L_0}$:
$$\kappa_0 \in \mathcal{Q}_0 = [-\bar{\kappa}_0, \bar{\kappa}_0], \tag{4}$$
where $\beta_0 \in [-\bar{\beta}_0, \bar{\beta}_0]$, $\bar{\beta}_0 \in (0, \pi/2)$ is the steering angle of the tractor's front wheels and $\bar{\kappa}_0 = \frac{\tan\bar{\beta}_0}{L_0}$ is the maximum curvature,
- and $S \in \{1, \ldots, N\}$ number of steering angles associated with actively steered trailers
$$\gamma_a \in \mathcal{Q}_a = [-\bar{\gamma}_a, \bar{\gamma}_a], \quad \bar{\gamma}_a \in (0, \pi/2), \tag{5}$$
where index $a \in \mathcal{I}_a \subseteq \{1, \ldots, N\}$ specifies which trailers that have steerable wheels. The control input for the MSNT with a car-like tractor is defined as
$$u = \left[\kappa_0 \ \boldsymbol{\gamma}_a^\mathsf{T}\right]^\mathsf{T} \in \mathcal{U}, \tag{6}$$
where κ_0 is the tractor's curvature and $\boldsymbol{\gamma}_a$ represents a vector of trailer steering angles and $\mathcal{U} = \mathcal{Q}_0 \times \underbrace{\mathcal{Q}_a \times \ldots \times \mathcal{Q}_a}_{S \text{ times}}$.

The leading car-like tractor is described by a kinematic single-track vehicle model and its orientation θ_0 evolves as
$$\dot{\theta}_0 = v_0 \kappa_0. \tag{7}$$
Between any two neighboring vehicle segments, the transformation of the angular $\dot{\theta}_i$ and longitudinal v_i velocities are given by (see, e.g., Michalek (2019)):
$$\begin{bmatrix}\dot{\theta}_i \\ v_i\end{bmatrix} = \underbrace{\begin{bmatrix} -\frac{M_i}{L_i}\frac{\cos(\beta_i - \gamma_i)}{\cos\gamma_i} & \frac{\sin(\beta_i - \gamma_i + \gamma_{i-1})}{L_i \cos\gamma_i} \\ M_i \frac{\sin\beta_i}{\cos\gamma_i} & \frac{\cos(\beta_i + \gamma_{i-1})}{\cos\gamma_i} \end{bmatrix}}_{\boldsymbol{J}_i(\beta_i, \gamma_i, \gamma_{i-1})} \begin{bmatrix}\dot{\theta}_{i-1} \\ v_{i-1}\end{bmatrix}, \tag{8}$$

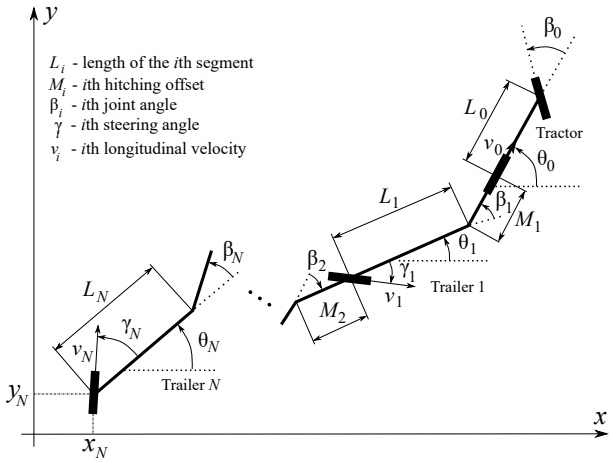

Fig. 1. A schematic description of the MSNT with a car-like tractor in a global coordinate system.

for $i = 1, \ldots, N$, where γ_i denotes the steering angle of the ith trailer. Note that if the jth trailer is passive, it suffices to take $\gamma_j = 0$, and that $\gamma_0 = 0$ because the tractor's rear wheel is non-steerable.

To satisfy actuator limitations, the rate of each trailer steering angle γ_a, $a \in \mathcal{I}_a$ and the tractor's curvature κ_0 are constrained as
$$\begin{aligned} |\dot{\gamma}_a| &\leq \dot{\bar{\gamma}}_a, \quad a \in \mathcal{I}_a, \\ |\dot{\kappa}_0| &\leq \dot{\bar{\kappa}}_0, \end{aligned} \tag{9}$$
which is compactly represented as $\dot{u} \in \Omega$. Moreover, the position of the Nth trailer evolves according to standard unicycle kinematics (see Fig. 1)
$$\begin{aligned} \dot{x}_N &= v_N \cos(\theta_N + \gamma_N), \\ \dot{y}_N &= v_N \sin(\theta_N + \gamma_N). \end{aligned} \tag{10}$$
Using (7) and (8), the angular rate $\dot{\theta}_N$ and longitudinal velocity v_N of the Nth trailer are given by
$$\begin{bmatrix}\dot{\theta}_N \\ v_N\end{bmatrix} = \prod_{i=0}^{N-1} \boldsymbol{J}_{N-i}(\beta_{N-i}, \gamma_{N-i}, \gamma_{N-i-1}) \begin{bmatrix} v_0\kappa_0 \\ v_0 \end{bmatrix}. \tag{11}$$
Note that v_0 enters bilinearly in (11). Therefore, using (11) and by introducing the vectors $c^\mathsf{T} = [1 \ 0]$ and $d^\mathsf{T} = [0 \ 1]$, the curvature of the Nth trailer is defined as
$$\kappa_N \triangleq \frac{\dot{\theta}_N}{v_N} = \frac{c^\mathsf{T} \prod_{i=0}^{N-1} \boldsymbol{J}_{N-i}(\beta_{N-i}, \gamma_{N-i}, \gamma_{N-i-1}) \begin{bmatrix}\kappa_0 \\ 1\end{bmatrix}}{f_{v_N}(\beta_1, \ldots, \beta_N, u)}, \tag{12}$$
where
$$f_{v_N} = d^\mathsf{T} \prod_{i=0}^{N-1} \boldsymbol{J}_{N-i}(\beta_{N-i}, \gamma_{N-i}, \gamma_{N-i-1}) \begin{bmatrix}\kappa_0 \\ 1\end{bmatrix}, \tag{13}$$
which relates the longitudinal velocity of the tractor and the Nth trailer $v_N = f_{v_N}(\beta_1, \ldots, \beta_N, u) v_0$. To guarantee that (12) is well defined, it is further assumed that the sets $\mathcal{X}$ and $\mathcal{U}$ are defined such that $f_{v_N} > 0$. Using (10), (11) and (13), the model for the pose of the Nth trailer can be represented as $\dot{q}_N = v_N f_{q_N}(x, u)$. Furthermore, using (7) and (8), the time derivative of (2) yields the joint-angle kinematics
$$\begin{aligned} \dot{\beta}_i = \dot{\theta}_{i-1} - \dot{\theta}_i = c^\mathsf{T} &\prod_{j=N-i+1}^{N-1} \boldsymbol{J}_{N-j}(\beta_{N-j}, \gamma_{N-j}, \gamma_{N-j-1}) \begin{bmatrix}\kappa_0 \\ 1\end{bmatrix} \frac{v_N}{f_{v_N}} \\ &- c^\mathsf{T} \prod_{j=N-i}^{N-1} \boldsymbol{J}_{N-j}(\beta_{N-j}, \gamma_{N-j}, \gamma_{N-j-1}) \begin{bmatrix}\kappa_0 \\ 1\end{bmatrix} \frac{v_N}{f_{v_N}}, \end{aligned} \tag{14}$$

for $i = 1, \dots, N$. Denote the joint-angle kinematics in (14) as $\dot{\beta}_i = v_N f_{\beta_i}(\beta_1, \dots, \beta_N, u)$, for $i = 1, \dots, N$. Now, the kinematic model of the MSNT vehicle with a car-like tractor is given in (10), (11) and (14), which can compactly be represented as

$$\dot{x} = v_N \boldsymbol{f}(x, u), \tag{15}$$

where $\boldsymbol{f} : \mathbb{R}^n \times \mathbb{R}^m \to \mathbb{R}^n$ is continuous and continuously differentiable with respect to $x \in \mathcal{X}$ and $u \in \mathcal{U}$.

3. PATH-FOLLOWING ERROR MODEL

It is assumed that a nominal trajectory $(x_r(\cdot), u_r(\cdot), v_{Nr}(\cdot))$ for the MSNT vehicle (15) is provided that satisfies the constraints on states $x_r(\cdot) \in \mathcal{X}$, and control inputs $u_r(\cdot) \in \mathcal{U}$ and $\dot{u}_r(\cdot) \in \Omega$. Given the vehicle's current state $x(t)$, define $s(t)$ as the distance traveled by the position of the Nth trailer onto its projection to its nominal path $(x_{Nr}(\cdot), y_{Nr}(\cdot))$ up to time t. By applying time-scaling (Sampei and Furuta, 1986), the nominal trajectory can instead be interpreted as a nominal path (Ljungqvist et al., 2019):

$$\frac{\mathrm{d}x_r}{\mathrm{d}s} = \bar{v}_{Nr} \boldsymbol{f}(x_r, u_r), \tag{16}$$

where $\bar{v}_{Nr} = \operatorname{sign}(v_{Nr}) \in \{-1, 1\}$ specifies the nominal motion direction. Similar to Ljungqvist et al. (2019), the idea is now to model the MSNT vehicle in terms of deviation from this nominal path, as illustrated in Fig. 2. Denote $\tilde{z}_N(t)$ as the signed lateral error between the position of the Nth trailer and its projection to its nominal path $(x_{Nr}(\cdot), y_{Nr}(\cdot))$. Denote the orientation error of the Nth trailer as $\tilde{\theta}_N(t) = \theta_N(t) - \theta_{Nr}(s(t))$ and define the joint-angle errors $\tilde{\beta}_i(t) = \beta_i(t) - \beta_{ir}(s(t))$, $i = 1, \dots, N$. Finally, define the control-input deviation as $\tilde{u}(t) = u(t) - u_r(s(t))$ and let $\kappa_{Nr} = \kappa_N(\beta_{1r}, \dots, \beta_{Nr}, u_r)$ represent the curvature of the nominal path for the Nth trailer. Using the Frenet-frame transformation together with the chain rule, the MSNT vehicle (15) can be described in terms of deviation from the nominal path (16) as

$$\dot{s} = v_N \frac{\bar{v}_{Nr} \cos(\tilde{\theta}_N + \tilde{\gamma}_N)}{1 - \kappa_{Nr} \tilde{z}_N}, \tag{17a}$$

$$\dot{\tilde{z}}_N = v_N \sin(\tilde{\theta}_N + \tilde{\gamma}_N), \tag{17b}$$

$$\dot{\tilde{\theta}}_N = v_N \left(\kappa_N(\tilde{\beta}_1 + \beta_{1r}, \dots, \tilde{\beta}_N + \beta_{Nr}, \tilde{u} + u_r) - \frac{\kappa_{Nr} \cos(\tilde{\theta}_N + \tilde{\gamma}_N)}{1 - \kappa_{Nr} \tilde{z}_N} \right), \tag{17c}$$

$$\dot{\tilde{\beta}}_i = v_N \left(f_{\beta_i}(\tilde{\beta}_1 + \beta_{1r}, \dots, \tilde{\beta}_N + \beta_{Nr}, \tilde{u} + u_r) - \frac{\cos(\tilde{\theta}_N + \tilde{\gamma}_N)}{1 - \kappa_{Nr} \tilde{z}_N} f_{\beta_i}(\beta_{1r}, \dots, \beta_{Nr}, u_r) \right), \tag{17d}$$

for $i = N, N-1, \dots, 1$. The transformation to the Frenet frame path-coordinate system is valid as long as $\tilde{z}_N$ and the sum $\tilde{\theta}_N + \tilde{\gamma}_N$ satisfy

$$1 - \kappa_{Nr}(s) \tilde{z}_N > 0, \quad |\tilde{\theta}_N + \tilde{\gamma}_N| < \pi/2. \tag{18}$$

Essentially, this gives that $|\tilde{z}_N| < |\kappa_{Nr}^{-1}(s)|$ must hold when $\tilde{z}_N$ and $\kappa_{Nr}(s)$ have the same sign. Note that $\bar{v}_{Nr}$ is included in (17a) to make $\dot{s} > 0$ as long as the constraints in (18) are satisfied, and the Nth trailer's velocity v_N and the nominal motion direction $\bar{v}_{Nr}$ have the same sign. Moreover, since it is assumed that $f_{v_N} > 0$ and the relationship $v_N = v_0 f_{v_N}(\beta_1, \dots, \beta_N, u)$ holds, an equivalent condition is that the velocity of the car-like tractor v_0 is selected such that $\operatorname{sign}(v_0) = \bar{v}_{Nr}$.

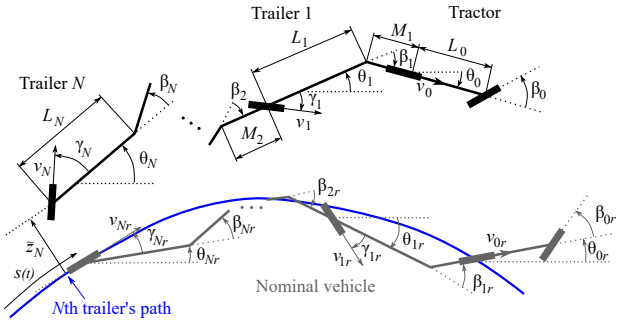

Fig. 2. A schematic description of the MSNT with a car-like tractor in the Frenet frame coordinate system.

Define the path-following error $\tilde{x} = \begin{bmatrix} \tilde{z}_N & \tilde{\theta}_N & \tilde{\beta}_N & \dots & \tilde{\beta}_1 \end{bmatrix}^\mathsf{T}$, where its model is given by (17b)–(17d). From the structure of (17b)–(17d), it is straightforward to verify that the origin $(\tilde{x}, \tilde{u}) = (0, 0)$ is an equilibrium point for all t. Moreover, since the velocity v_0 of the tractor is selected such that $\dot{s}(t) > 0$, it is possible to perform time-scaling (Sampei and Furuta, 1986) and eliminate the time-dependency presented in (17b)–(17d). Using the chain rule, it holds that $\frac{\mathrm{d}\tilde{x}}{\mathrm{d}s} = \frac{\mathrm{d}\tilde{x}}{\mathrm{d}t} \frac{1}{\dot{s}}$, and the spatial version of the path-following error model (17b)–(17d) becomes

$$\frac{\mathrm{d}\tilde{z}_N}{\mathrm{d}s} = \bar{v}_{Nr}(1 - \kappa_{Nr} \tilde{z}_N) \tan(\tilde{\theta}_N + \tilde{\gamma}_N), \tag{19a}$$

$$\frac{\mathrm{d}\tilde{\theta}_N}{\mathrm{d}s} = \bar{v}_{Nr} \left(\frac{1 - \kappa_{Nr} \tilde{z}_N}{\cos(\tilde{\theta}_N + \tilde{\gamma}_N)} \kappa_N(\tilde{\beta}_1 + \beta_{1r}, \dots, \tilde{\beta}_N + \beta_{Nr}, \tilde{u} + u_r) - \kappa_{Nr} \right), \tag{19b}$$

$$\frac{\mathrm{d}\tilde{\beta}_i}{\mathrm{d}s} = \bar{v}_{Nr} \left(\frac{1 - \kappa_{Nr} \tilde{z}_N}{\cos(\tilde{\theta}_N + \tilde{\gamma}_N)} f_{\beta_i}(\tilde{\beta}_1 + \beta_{1r}, \dots, \tilde{\beta}_N + \beta_{Nr}, \tilde{u} + u_r) - f_{\beta_i}(\beta_{1r}, \dots, \beta_{Nr}, u_r) \right), \quad i = N, N-1, \dots, 1, \tag{19c}$$

which can be compactly represented as

$$\frac{\mathrm{d}\tilde{x}}{\mathrm{d}s} = \bar{v}_{Nr} \tilde{\boldsymbol{f}}(s, \tilde{x}, \tilde{u}), \tag{20}$$

where $\tilde{\boldsymbol{f}}(s, 0, 0) = 0$ for all s. In the next section, a model predictive path-following controller is proposed to stabilize the path-following error model (20) around the origin, i.e., around the nominal path (16).

4. MODEL PREDICTIVE PATH-FOLLOWING CONTROLLER

The objective of the model predictive path-following controller is to control the tractor's curvature κ_0 and the trailer steering angles $\boldsymbol{\gamma}_a$ such that the path-following error is minimized, while the constraints on states $x \in \mathcal{X}$, and control inputs $u \in \mathcal{U}$ and $\dot{u} \in \Omega$ are satisfied for all time instances. To obtain an MPC problem that can be solved online at a high sampling rate, the goal is to derive an MPC formulation that can be converted into the form of a quadratic programming (QP) problem. First, the nonlinear path-following error model (20) is linearized around the origin $(\tilde{x}, \tilde{u}) = (0, 0)$, i.e., around the nominal path:

$$\frac{\mathrm{d}\tilde{x}}{\mathrm{d}s} = \bar{v}_{Nr} \boldsymbol{A}(s) \tilde{x} + \bar{v}_{Nr} \boldsymbol{B}(s) \tilde{u}, \tag{21}$$

where $\tilde{x}$ is the path-following error and $\tilde{u}$ is the control-input deviation. Using Euler-forward discretization with sampling distance Δ_s, the discrete-time approximation of (21) becomes

$$\tilde{x}_{k+1} = \boldsymbol{F}_k \tilde{x}_k + \boldsymbol{G}_k \tilde{u}_k, \tag{22}$$

where

$$\boldsymbol{F}_k = \boldsymbol{I} + \Delta_s \bar{v}_{Nr} \boldsymbol{A}_k, \quad \boldsymbol{G}_k = \Delta_s \bar{v}_{Nr} \boldsymbol{B}_k. \tag{23}$$

Since the tractor's curvature and the trailer-steering angles are $u_k = \tilde{u}_k + u_{r,k} \in \mathcal{U}$, they are bounded as

$$-\bar{u}_k \leq \tilde{u}_k + u_{r,k} \leq \bar{u}_k, \tag{24}$$

where $\bar{u}_k = \begin{bmatrix} \bar{\kappa}_{0,k} & \bar{\boldsymbol{\gamma}}_{a,k}^\intercal \end{bmatrix}^\intercal$ and $\bar{\boldsymbol{\gamma}}_{a,k}$ represents a vector of maximum trailer-steering angles. Furthermore, since $\dot{s} > 0$ and $v_N = v_0 f_{v_N}(\beta_1, \dots, \beta_N, u)$, the rate limits on the control input $\dot{u} \in \Omega$ can be described in s using the chain rule as

$$\begin{aligned} \left| \frac{\mathrm{d}\kappa_0}{\mathrm{d}s} \right| &\leq \frac{\dot{\bar{\kappa}}_0}{\dot{s}} = \frac{1 - \kappa_{Nr} \tilde{z}_N}{|v_0| f_{v_N}(\beta_1, \dots, \beta_N, u) \cos(\tilde{\theta}_N + \tilde{\gamma}_N)} \dot{\bar{\kappa}}_0, \\ \left| \frac{\mathrm{d}\gamma_a}{\mathrm{d}s} \right| &\leq \frac{\dot{\bar{\gamma}}_a}{\dot{s}} = \frac{1 - \kappa_{Nr} \tilde{z}_N}{|v_0| f_{v_N}(\beta_1, \dots, \beta_N, u) \cos(\tilde{\theta}_N + \tilde{\gamma}_N)} \dot{\bar{\gamma}}_a, \end{aligned} \tag{25}$$

for $a \in \mathcal{I}_a$. Locally around the origin $(\tilde{x}, \tilde{u}) = (0, 0)$, it holds that $\cos(\tilde{\theta}_N + \tilde{\gamma}_N) \approx 1$ and $\kappa_{Nr} \tilde{z}_N \approx 0$. Therefore, to avoid coupling between $\tilde{u}$ and $\tilde{x}$, the constraints in (25) are approximated as

$$\begin{aligned} \left| \frac{\mathrm{d}\kappa_0}{\mathrm{d}s} \right| &\leq \frac{\dot{\bar{\kappa}}_0}{|v_0| f_{v_N}(\beta_{1r}, \dots, \beta_{Nr}, u_r)} \triangleq \bar{c}_0(s), \\ \left| \frac{\mathrm{d}\gamma_a}{\mathrm{d}s} \right| &\leq \frac{\dot{\bar{\gamma}}_a}{|v_0| f_{v_N}(\beta_{1r}, \dots, \beta_{Nr}, u_r)} \triangleq \bar{c}_a(s), \quad a \in \mathcal{I}_a. \end{aligned} \tag{26}$$

By discretizing (26) using Euler forward with sampling distance Δ_s, the rate limits on the control input can be described by the following slew-rate constraint

$$-\bar{\boldsymbol{c}}_k \Delta_s \leq \tilde{u}_k - \tilde{u}_{k-1} - \bar{u}_{r,k} \leq \bar{\boldsymbol{c}}_k \Delta_s, \tag{27}$$

where $\bar{u}_{r,k} = u_{r,k} - u_{r,k-1}$ and $\bar{\boldsymbol{c}}_k = \begin{bmatrix} \bar{c}_{0,k} & \bar{\boldsymbol{c}}_{a,k}^\intercal \end{bmatrix}^\intercal$, where $\bar{\boldsymbol{c}}_{a,k}$ represents a vector of rate limits for the trailer-steering angles. Denote the linear inequality constraints in (24) and (27) as $\tilde{u}_k \in \tilde{\mathcal{U}}_k$. Finally, since $\beta_{i,k} = \beta_{ir,k} + \tilde{\beta}_{i,k}$, $i = 1, \dots, N$, the constraints on the joint angles can be written as

$$-\bar{\beta}_i \leq \beta_{ir,k} + \tilde{\beta}_{i,k} \leq \bar{\beta}_i, \quad i = 1, \dots, N, \tag{28}$$

which is compactly denoted as $\tilde{x}_k \in \tilde{\mathcal{X}}_k$. Note that $\tilde{\mathcal{X}}_k$ can be designed to also include constraints on other path-following error states. Now, given the path-following error $\tilde{x}(s(t))$ at time t, the MPC problem with prediction horizon $\bar{N}$ is defined as follows

$$\begin{aligned} \underset{\tilde{\mathbf{x}}, \tilde{\boldsymbol{u}}}{\text{minimize}} \quad & V_{\bar{N}}(\tilde{\mathbf{x}}, \tilde{\boldsymbol{u}}) = V_f(\tilde{x}_{\bar{N}}) + \sum_{k=0}^{\bar{N}-1} l(\tilde{x}_k, \tilde{u}_k) \\ \text{subject to} \quad & \tilde{x}_{k+1} = \boldsymbol{F}_k \tilde{x}_k + \boldsymbol{G}_k \tilde{u}_k, \; k = 0, \dots, \bar{N} - 1, \\ & \tilde{x}_k \in \tilde{\mathcal{X}}_k, \quad \tilde{u}_k \in \tilde{\mathcal{U}}_k, \quad k = 0, \dots, \bar{N} - 1, \\ & \tilde{x}_0 = \tilde{x}(s(t)) \text{ given}, \end{aligned} \tag{29}$$

where $\tilde{\mathbf{x}}^\intercal = [\tilde{x}_0^\intercal \; \tilde{x}_1^\intercal \; \dots \; \tilde{x}_{\bar{N}}^\intercal]$ is the predicted path-following error sequence and $\tilde{\mathbf{u}}^\intercal = [\tilde{u}_0^\intercal \; \tilde{u}_1^\intercal \; \dots \; \tilde{u}_{\bar{N}-1}^\intercal]$ is the control-input deviation sequence. The stage-cost is chosen to be quadratic $l(\tilde{x}_k, \tilde{u}_k) = ||\tilde{x}_k||_{\boldsymbol{Q}}^2 + ||\tilde{u}_k||_{\boldsymbol{R}}^2$ as well as and the terminal cost $V_f(\tilde{x}_{\bar{N}}) = \tilde{x}_{\bar{N}}^\intercal \boldsymbol{P}_{\bar{N}} \tilde{x}_{\bar{N}}$, where the matrices $\boldsymbol{Q} \succeq 0$, $\boldsymbol{R} \succ 0$ and $\boldsymbol{P}_{\bar{N}} \succ 0$ are design choices. Since the cost function $V_{\bar{N}}$ is quadratic and there are only linear equality and inequality constraints, the optimization problem in (29) can be written as a standard QP problem. Thus, at each sampling instance, the QP problem in (29) is solved to obtain the optimal open-loop control-input deviation sequence $\tilde{\boldsymbol{u}}^*$. Only the first control-input deviation $\tilde{u}_0^*$ is deployed to the vehicle

$$u(t) = u_r(s(t)) + \tilde{u}_0^*, \tag{30}$$

and the QP problem (29) is repeatedly solved at a fixed controller frequency f_s using the current state estimate. Note that the MPC controller only computes the feedback part of the control input $\tilde{u}_0^*$, as the optimal feedforward $u_r(s(t))$ already is provided by the motion planner.

4.1 Controller design

We now turn to the problem of designing the cost function $V_{\bar{N}}$ for the MPC controller (29). Since the nominal path contains full state and control-input information, it is possible to compute the nominal path as well as the nominal orientation of each vehicle segment using holonomic relationships (Altafini, 2001). In order to minimize the risk of colliding with any obstacle, it is preferred that the MPC controller is tuned such that all path-following errors are penalized. Denote $\tilde{z}_i$, $i = 0, \dots, N-1$ as the lateral error of the ith vehicle segment with respect to its nominal path, and denote $\tilde{\theta}_i = \theta_i - \theta_{ir}$, $i = 0, \dots, N-1$ as their corresponding heading errors. As explained in Altafini (2003), it is for general paths not possible to derive closed-form expressions to relate these auxiliary path-following errors as a function of the modeled ones $\tilde{x}$. However, around a straight nominal path, closed-form expressions exist and the lateral and heading errors can be described as a function of $\tilde{x}$ using the following recursion

$$\begin{aligned} \tilde{z}_i &= \tilde{z}_{i+1} + L_{i+1} \sin \tilde{\theta}_{i+1} + M_{i+1} \sin(\tilde{\theta}_{i+1} + \tilde{\beta}_{i+1}), \\ \tilde{\theta}_i &= \tilde{\theta}_{i+1} + \tilde{\beta}_{i+1}, \quad i = N-1, \dots, 0. \end{aligned} \tag{31}$$

Using these approximate relationships also for curved nominal paths, define

$$\boldsymbol{z} = [\tilde{x}^\intercal \; \tilde{z}_{N-1} \; \tilde{\theta}_{N-1} \; \dots \; \tilde{z}_0 \; \tilde{\theta}_0]^\intercal \triangleq \boldsymbol{h}_z(\tilde{x}), \tag{32}$$

where $\boldsymbol{h}_z(0) = 0$, which defines the control-objective vector intended to be penalized. Since $\boldsymbol{h}_z(\tilde{x})$ in nonlinear, it is linearized around the origin which yields $\boldsymbol{z} = \frac{\partial \boldsymbol{h}_z(0)}{\partial \tilde{x}} \tilde{x} \triangleq \boldsymbol{M} \tilde{x}$. The matrix $\boldsymbol{M}$ is then used to select the weight matrix for the quadratic stage-cost on $\tilde{x}$ as $\boldsymbol{Q} = \boldsymbol{M}^\intercal \bar{\boldsymbol{Q}} \boldsymbol{M}$, where $\bar{\boldsymbol{Q}} \succeq 0$ is a diagonal design matrix. Now, each diagonal element in $\bar{\boldsymbol{Q}}$ penalizes a specific control objective in $\boldsymbol{z}$. The matrix $\boldsymbol{M}$ is then used to transform the specified design choice to $\boldsymbol{Q}$, which typically obtains nonzero off-diagonal elements.

When the matrices $\boldsymbol{Q}$ and $\boldsymbol{R}$ are selected, the weight matrix for the terminal cost $\boldsymbol{P}_{\bar{N}} \succ 0$ is computed by solving the discrete-time algebraic Riccati equation (DARE):

$$\boldsymbol{P}_{\bar{N}} = \boldsymbol{F}^\intercal \boldsymbol{P}_{\bar{N}} \boldsymbol{F} + \boldsymbol{Q}_1 - \boldsymbol{F}^\intercal \boldsymbol{P}_{\bar{N}} \boldsymbol{G} \boldsymbol{K}, \tag{33}$$

where $\boldsymbol{K} = (\boldsymbol{R} + \boldsymbol{G}^\intercal \boldsymbol{P}_{\bar{N}} \boldsymbol{G})^{-1} \boldsymbol{G}^\intercal \boldsymbol{P}_{\bar{N}} \boldsymbol{F}$ is the linear quadratic (LQ) feedback gain, and $\boldsymbol{F}$ and $\boldsymbol{G}$ are the discrete system matrices (23) for the linearized path-following error model (21) around a straight nominal path. Note that since the nominal motion direction $\bar{v}_{Nr} \in \{-1, 1\}$ enters bilinearly in (21), the system's stability properties depend on the nominal motion direction. As a consequence, different terminal costs are used during backward and forward motion tasks (Ljungqvist et al., 2019; Altafini et al., 2001). Moreover, since the prediction model used in the MPC

controller is an approximation, the originally hard joint-angle constraints are replaced with soft constraints using standard techniques (Mayne et al., 2000).

Even though there exists a well-established theory for guaranteeing closed-loop stability for MPC (see e.g. Mayne et al. (2000); Garcia et al. (1989)), a formal stability analysis is out of the scope in this work. Instead, extensive simulations are included to indicate the performance and stability properties of the MSNT vehicle using the proposed MPC controller (29).

5. SIMULATION RESULTS

In this section, the proposed model predictive path-following controller is evaluated on a MS2T with a car-like tractor, where trailer $N = 2$ is steerable, i.e., $\mathcal{I}_a = \{2\}$, and a mixture of off-axle ($M_1 \neq 0$) and on-axle ($M_2 = 0$) hitch connections. The vehicle parameters are presented in Table 1. Except for that trailer 2 is steerable, the parameters coincide with the full-scale test platform presented in Ljungqvist et al. (2019). Using the formulas presented in Section 2, it is now straightforward to derive the kinematic vehicle model (15) with state vector $x^\intercal = [x_2 \;\; y_2 \;\; \theta_2 \;\; \beta_2 \;\; \beta_1]$ and control input $u^\intercal = [\kappa_0 \;\; \gamma_2]$. Moreover, the path-following error is $\tilde{x}^\intercal = \begin{bmatrix}\tilde{z}_2 & \tilde{\theta}_2 & \tilde{\beta}_2 & \tilde{\beta}_1\end{bmatrix}$ and the control-input deviation is $\tilde{u}^\intercal = [\tilde{\kappa}_0 \;\; \tilde{\gamma}_2]$. Using the recursive formulas presented in Section 2 and Section 3 for this specific MS2T vehicle, the spatial path-following error model (20) becomes

$$
\begin{aligned}
\frac{\mathrm{d}\tilde{z}_2}{\mathrm{d}s} &= \bar{v}_{2r}(1-\kappa_{2r}\tilde{z}_2)\tan(\tilde{\theta}_2+\tilde{\gamma}_2),\\
\frac{\mathrm{d}\tilde{\theta}_2}{\mathrm{d}s} &= \bar{v}_{2r}\left(\frac{1-\kappa_{2r}\tilde{z}_2}{\cos(\tilde{\theta}_2+\tilde{\gamma}_2)}\kappa_2(\beta_{2r}+\tilde{\beta}_2,\gamma_{2r}+\tilde{\gamma}_2)-\kappa_{2r}\right),\\
\frac{\mathrm{d}\tilde{\beta}_2}{\mathrm{d}s} &= \bar{v}_{2r}\Bigg(\frac{1-\kappa_{2r}\tilde{z}_2}{\cos(\tilde{\theta}_2+\tilde{\gamma}_2)}f_{\beta_2}(\beta_{1r}+\tilde{\beta}_1,\beta_{2r}+\tilde{\beta}_2,u_r+\tilde{u})\\
&\qquad - f_{\beta_2}(\beta_{1r},\beta_{2r},u_r)\Bigg),\\
\frac{\mathrm{d}\tilde{\beta}_1}{\mathrm{d}s} &= \bar{v}_{2r}\Bigg(\frac{1-\kappa_{2r}\tilde{z}_2}{\cos(\tilde{\theta}_2+\tilde{\gamma}_2)}f_{\beta_1}(\beta_{1r}+\tilde{\beta}_1,\beta_{2r}+\tilde{\beta}_2,u_r+\tilde{u})\\
&\qquad - f_{\beta_1}(\beta_{1r},\beta_{2r},u_r)\Bigg),
\end{aligned}
\tag{34}
$$

where $\kappa_{2r} = \kappa_2(\beta_{2r}, \gamma_{2r})$ is the nominal curvature of trailer 2, and the functions f_{β_1}, f_{β_2} and κ_2 are provided in Appendix A. The model in (34) can compactly be written as $\mathrm{d}\tilde{x}/\mathrm{d}s = \bar{v}_{2r}\tilde{\boldsymbol{f}}(s,\tilde{x},\tilde{u})$, and its linearization around the origin $(\tilde{x},\tilde{u}) = (0,0)$ can be written as in (21), where the matrices $\boldsymbol{A}(s)$ and $\boldsymbol{B}(s)$ are provided in Appendix A. The linearized system (21) is then discretized using a sampling distance $\Delta_s = 0.2$ m to obtain a discrete-time representation (22).

The proposed MPC controller is designed following the approach presented in Section 4, where the design parameters are listed in Table 2 and the control-objective vector is $\boldsymbol{z}^\intercal = \begin{bmatrix}\tilde{x}^\intercal & \tilde{z}_1 & \tilde{\theta}_1 & \tilde{z}_0 & \tilde{\theta}_0\end{bmatrix}$. The terminal costs $\boldsymbol{P}_{\bar{N}}$ (one for forward and one for backward motion tasks) are computed by solving the DARE in (33) using the discrete system matrices $\boldsymbol{F} = \boldsymbol{I} + \Delta_s\bar{v}_{2r}\boldsymbol{A}$ and $\boldsymbol{G} = \Delta_s\bar{v}_{2r}\boldsymbol{B}$, obtained around a straight nominal path in forward ($\bar{v}_{2r} = 1$) and backward ($\bar{v}_{2r} = -1$) motion. The matrices $\boldsymbol{A}$ and $\boldsymbol{B}$ are provided in Appendix A.

Table 1. Vehicle parameters for the MS2T vehicle.

Vehicle parameter	Value
Tractor's wheelbase L_0	4.62 m
Length of off-hitch M_1	1.66 m
Length of trailer 1 L_1	3.87 m
Length of trailer 2 L_2	8.0 m
Maximum joint angles $\bar{\beta}_i$, $i = 1, 2$	0.8 rad
Maximum curvature of tractor $\bar{\kappa}_0$	0.18 m^{-1}
Maximum curvature rate of tractor $\dot{\bar{\kappa}}_0$	0.13 $\mathrm{m}^{-1}\mathrm{s}^{-1}$
Maximum steering angle trailer 2 $\bar{\gamma}_3$	0.35 rad
Maximum steering-angle rate trailer 2 $\dot{\bar{\gamma}}_2$	0.8 rad/s

The MPC controller is implemented in Matlab using YALMIP where Gurobi 8.1.1 is used as QP solver (Gurobi Optimization, 2019) to solve (29) at each sampling instance. The performance of the proposed MPC controller is evaluated in a simulation study containing a straight and a figure-eight nominal path. The simulations are performed on a standard laptop computer with an Intel Core i7-4600U@2.1GHz CPU. The proposed MPC controller (MS2T-MPC) is benchmarked with an LQ controller (MS2T-LQ), as proposed in Ljungqvist et al. (2019). The LQ controller is given by $\tilde{u} = \boldsymbol{K}\tilde{x}$, where the feedback gain $\boldsymbol{K}$ is computed by solving the DARE in (33) using the weight matrices $\boldsymbol{Q}$ and $\boldsymbol{R}$ that are also used by the MPC controller. Additionally, to analyze if the MPC controller is able to exploit the additional steering capability, it is also compared with an MPC controller for an SS2T vehicle, i.e., $\bar{\gamma}_2 = 0$, with the same vehicle parameters. This MPC controller (SS2T-MPC) uses the same design parameters except that the weight matrix on the control-input deviation is selected as $\boldsymbol{R} = 4$, because the control input $\tilde{u} = \tilde{\kappa}_0$ is a scalar for SS2T. Moreover, to make fair comparisons the nominal paths are designed to be feasible for the SS2T vehicle, i.e., $\gamma_{2r} = 0$. In the simulations, the initial path-following error $\tilde{x}^i = \tilde{x}(0)$ is perturbed to compare how the different controllers handle disturbance rejection while satisfying the constraints on the joint angles.

The first set of simulations involves backward tracking of a straight nominal path aligned with the x-axis, where the longitudinal velocity of the tractor is selected as $v_0 = -1$ m/s. In this scenario, the initial state is $\tilde{x}^i = \begin{bmatrix}0 & 0 & \beta_2^i & \beta_1^i\end{bmatrix}^\intercal$, where the initial joint-angle errors β_2^i and β_1^i are perturbed to various degrees. First, to analyze the stability region of the closed-loop systems, we numerically compute the region of attraction for the systems by performing simulations from a large set of initial joint-angle errors. In these simulations, the joint-angle constraints are temporarily removed from the MPC controllers and the closed-systems are checked for convergence to the straight nominal path. The resulting regions obtained from simulations are illustrated in Fig. 3c. As expected, MS2T-MPC (blue set) has the largest region. Even though SS2T-MPC has non-steerable trailers, its region of attraction (red set) is larger than for MS2T-LQ (green set). This result is obtained because the LQ

Table 2. Design parameters for the MPC controller.

Vehicle parameter	Value
Prediction horizon $\bar{N}$	40
Weight matrix $\bar{\boldsymbol{Q}}$	$1/35 \times \mathrm{diag}([0.5 \;\; 1 \;\; 4 \;\; 4 \;\; 0.5 \;\; 1 \;\; 0.5 \;\; 1])$
Weight matrix $\boldsymbol{R}$	$\mathrm{diag}([4 \;\; 3])$
Sampling distance Δ_s	0.2 m
Controller frequency f_s	10 Hz

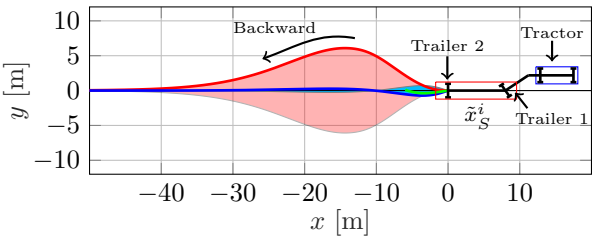

(a) The envelopes of the trajectories for the position of trailer 2 during backward tracking of a straight path (black line), using SS2T-MPC (red set) and MS2T-MPC (blue set). For the high-lighted initial state $\tilde{x}_S^i$, MS2T-LQ leads to jack-knife (see Fig. 3b.).

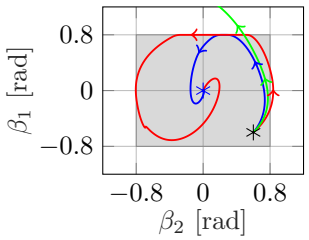

(b) The joint-angle trajectories from initial state $\tilde{x}_S^i$ in Fig. 3a. Initial (desired) state denoted by a black (blue) star.

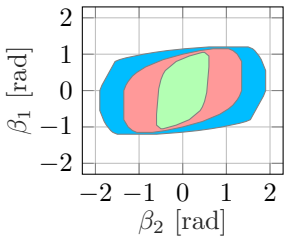

(c) The simulated stability regions for MS2T-LQ (green set), SS2T-MPC (red set) and MS2T-MPC (blue set).

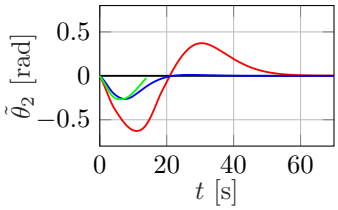

(d) Heading error of trailer 2 from initial state $\tilde{x}_S^i$.

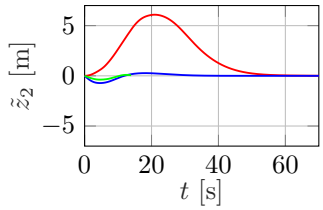

(e) Lateral error of trailer 2 from initial state $\tilde{x}_S^i$.

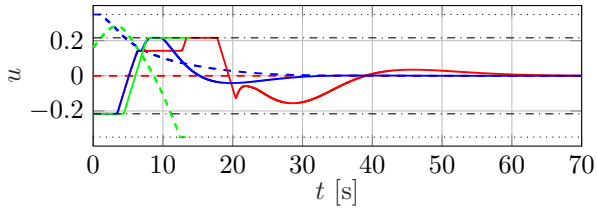

(f) Control input $u^\intercal = [\kappa_0 \;\; \gamma_2]$ from $\tilde{x}_S^i$. κ_0 (solid) and γ_2 (dashed) and their limits $\bar{\kappa}_0$ (dashed-dotted black) and $\bar{\gamma}_2$ (dotted black).

Fig. 3. Path following of a straight nominal path ($y_{3r} = 0$) in backward motion from perturbed initial joint-angle errors $\tilde{\beta}_1^i, \tilde{\beta}_2^i \in [-0.6, 0.6]$ rad, using MS2T-LQ (green lines), SS2T-MPC (red lines) and MS2T-MPC (blue lines). High-lighted initial state $\tilde{x}_S^i$ in Fig. 3a is for $(\beta_2^i, \beta_1^i) = (0.6, -0.6)$ rad. In Fig. 3b, the gray box illustrates the used joint-angle constraints.

controller is not aware of the control-input constraints, as opposed to the two MPC controllers.

The envelopes of the trajectories for position $(x_2(\cdot), y_2(\cdot))$ using MS2T-MPC and SS2T-MPC with initial joint-angle errors $\tilde{\beta}_1^i, \tilde{\beta}_2^i \in [-0.6, 0.6]$ rad, are illustrated in Fig. 3a [1]. The transient response for MS2T-MPC yields a significantly smaller maximum overshoot in the lateral error of trailer 2 (0.26 m) compared to SS2T-MPC (6.1 m). The reason for this can be seen in Fig. 3f, where the control-input trajectories are plotted from initial state $\tilde{x}_S^i$ with $(\tilde{\beta}_2^i, \tilde{\beta}_1^i) = (0.6, -0.6)$ rad. The results show that MS2T-MPC uses a positive trailer-steering angle γ_2 (blue dashed line) to compensate for the initially positive value of β_2 (see Fig. 3b). The trailer-steering angle is also used by MS2T-MPC to reduce the maximum overshoot in the heading error of trailer 2 (0.26 rad) compared to SS2T-MPC (0.62 rad) (see Fig. 3d). Moreover, the joint-angle trajectories from initial state $\tilde{x}_S^i$ are plotted in Fig. 3b. As can be seen, MS2T-LQ is not able to stabilize the vehicle due to the input constraints and jackknifing occurs almost instantly. As a comparison, both MPC controllers are able to make the system converge to the straight nominal path, but SS2T-MPC has to initially violate the soft joint-angle constraints, which is not the case for MS2T-MPC.

The second set of simulations involves backward tracking ($v_0 = -1$ m/s) and forward tracking ($v_0 = 1$ m/s) of a figure-eight nominal path in $(x_{2r}(\cdot), y_{2r}(\cdot))$, which has been computed as described in Ljungqvist et al. (2019). Also in this set of simulations, the initial state $\tilde{x}(0)$ is perturbed to compare the performance of the controllers. The simulation results are presented in Fig. 4. Scenario A involves a heading error $\tilde{\theta}_2^i \in [-1, 1]$ rad and Scenario B a lateral error $\tilde{z}_2^i \in [-5, 5]$ m, both in backward motion. As for the first set of simulations, the MS2T-MPC uses the trailer-steering angle to reduce the overshoot and convergence times for $\tilde{z}_2$ and $\tilde{\theta}_2$ compared to SS2T-MPC (see, e.g., Fig. 4d–4e). Moreover, MS2T-LQ is not able to stabilize the system and jack-knife occurs almost instantly from some initial states, e.g., $\tilde{x}_{A1}^i$ with $\tilde{\theta}_2^i = -1$ rad (see Fig. 4b) and $\tilde{x}_{B1}^i$ with $\tilde{z}_2^i = -5$ m. Finally, Scenario C involves both a lateral $\tilde{z}_2^i \in [-2, 2]$ m and an initial heading error $\tilde{\theta}_2^i \in [-0.3, 0.3]$ rad in forward motion. As can be seen in Fig. 4a, the envelope of the trajectories $(x_2(\cdot), y_2(\cdot))$ is smallest for MS2T-LQ (green set). The joint-angle trajectories (see Fig. 4c) in the MS2T-LQ case are however drastically violating their constraints at some parts of the maneuvers, which is neither the case for MS2T-MPC nor SS2T-MPC. As a final note, the average computation time in Gurobi for the proposed MS2T-MPC is 35 ms compared to 25 ms for SS2T-MPC which is less than the sampling time $T_s = 100$ ms of the controllers.

6. CONCLUSIONS

A model predictive path-following controller is proposed for multi-steered articulated vehicles composed of a car-like tractor and an arbitrary number of off/on-axle hitched trailers with steerable/non-steerable wheels. The proposed MPC controller uses a path-following error model of the vehicle for predictions, is designed to satisfy physically constraints on states and control inputs, and is tailored to follow nominal paths that contain full state and control-input information. The performance of the proposed path-following controller is evaluated in a set of practically relevant scenarios for a multi-steered 2-trailer with a car-like tractor where the last trailer is steerable. In simulations, it is shown that the proposed controller outperforms a linear quadratic controller and efficiently exploits the additional trailer-steering capability, while recovering from non-trivial initial states in backward motion.

As future work, we would like develop a motion planner and evaluate the framework in real-work experiments on a full-scale test vehicle.

[1] The envelope for MS2T-LQ is not presented in Fig. 3a since the vehicle enters a jack-knife state for some $\tilde{\beta}_1^i, \tilde{\beta}_2^i \in [-0.6, 0.6]$, e.g., from the initial state $\tilde{x}_S^i$ with $(\beta_2^i, \beta_1^i) = (0.6, -0.6)$ rad.

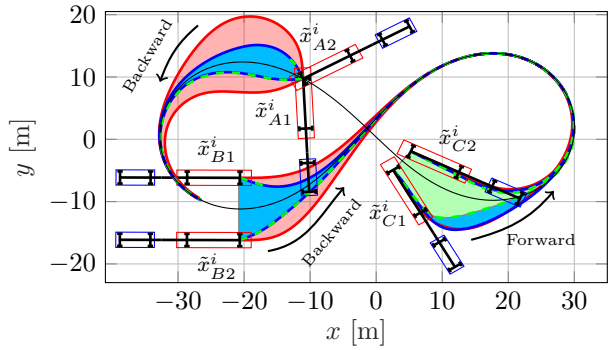

(a) The envelopes of the trajectories for the position of trailer 2 during backward and forward tracking of a figure-eight nominal path in $(x_{2r}(\cdot), y_{2r}(\cdot))$ (black line), using MS2T-LQ (green sets), SS2T-MPC (red sets) and MS2T-MPC (blue sets). For some highlighted initial states, MS2T-LQ leads to jack-knife (see Fig. 4b.).

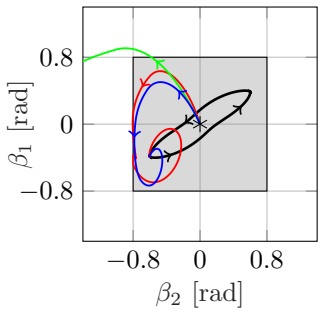

(b) Joint-angle trajectories from high-lighted initial state $\tilde{x}^i_{A1}$ in Fig. 4a. Initial state denoted by black star and nominal path $(\beta_{1r}(\cdot), \beta_{2r}(\cdot))$ by black line.

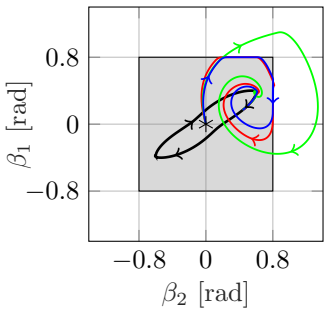

(c) Joint-angle trajectories from high-lighted initial state $\tilde{x}^i_{C1}$ in Fig. 4a. Initial state denoted by black star and nominal path in $(\beta_{1r}(\cdot), \beta_{2r}(\cdot))$ by black line.

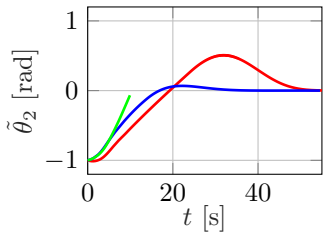

(d) Heading error of trailer 2 from initial state $\tilde{x}^i_{A1}$.

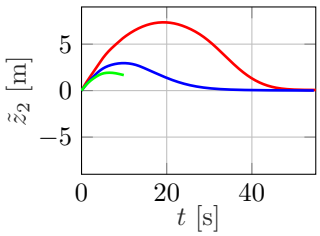

(e) Lateral error of trailer 2 from initial state $\tilde{x}^i_{A1}$.

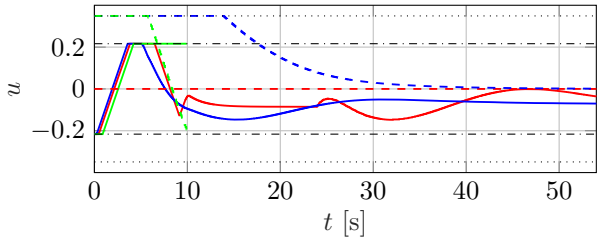

(f) Control input $u^\mathsf{T} = [\kappa_0 \;\; \gamma_2]$ from $\tilde{x}^i_{A1}$. κ_0 (solid) and γ_2 (dashed) and their limits $\bar{\kappa}_0$ (dashed-dotted black) and $\bar{\gamma}_2$ (dotted black).

Fig. 4. Path following of a figure-eight path in backward (Scenario A and Scenario B) and in forward motion (Scenario C) from perturbed initial states using MS2T-LQ (green lines), SS2T-MPC (red lines) and MS2T-MPC (blue lines). In Scenario A (see Fig. 4), heading error $\tilde{\theta}^i_2 \in [-1, 1]$ rad, in Scenario B, lateral error $\tilde{z}^i_2 \in [-5, 5]$ m and in Scenario C, both lateral error $\tilde{z}^i_2 \in [-2, 2]$ m and heading error $\tilde{\theta}^i_2 \in [-0.3, 0.3]$ rad. In Fig. 4b-4c, the gray box illustrates the joint-angle constraints.

APPENDIX A

We start by deriving the functions f_{β_1}, f_{β_2} and κ_2 describing the path-following error model for the specific MS2T with a car-like tractor (34). The matrices $\boldsymbol{J}_1$ and $\boldsymbol{J}_2$ describing the longitudinal and angular velocity transformations between neighboring vehicle segments (8) are

$$\begin{aligned}\boldsymbol{J}_1(\beta_1, 0, 0) &= \begin{bmatrix} -\dfrac{M_1}{L_1}\cos\beta_1 & \dfrac{\sin\beta_1}{L_1} \\ M_1 \sin\beta_1 & \cos\beta_1 \end{bmatrix}, \\ \boldsymbol{J}_2(\beta_2, \gamma_2, 0) &= \begin{bmatrix} 0 & \dfrac{\sin(\beta_2 - \gamma_2)}{L_2 \cos\gamma_2} \\ 0 & \dfrac{\cos\beta_2}{\cos\gamma_2} \end{bmatrix},\end{aligned} \tag{35}$$

since $M_2 = \gamma_0 = \gamma_1 = 0$. Thus, the velocity transformation from trailer 2 to the car-like tractor (13) is

$$f_{v_2}(\beta_1, \beta_2, u) = d^\mathsf{T} \boldsymbol{J}_2 \boldsymbol{J}_1 \begin{bmatrix} \kappa_0 \\ 1 \end{bmatrix} = \frac{\cos\beta_2}{\cos\gamma_2}\left(M_1 \sin\beta_1 \kappa_0 + \cos\beta_1\right), \tag{36}$$

and the curvature of trailer 2 (12) is

$$\kappa_2(\beta_2, \gamma_2) = \frac{c^\mathsf{T} \boldsymbol{J}_2 \boldsymbol{J}_1 \begin{bmatrix} \kappa_0 \\ 1 \end{bmatrix}}{d^\mathsf{T} \boldsymbol{J}_2 \boldsymbol{J}_1 \begin{bmatrix} \kappa_0 \\ 1 \end{bmatrix}} = \frac{\sin(\beta_2 - \gamma_2)}{L_2 \cos\beta_2}. \tag{37}$$

Finally, using (35)–(37) the functions describing the joint-angle kinematics (14) are

$$\begin{aligned} f_{\beta_2}(\beta_1, \beta_2, u) =& \frac{\cos\gamma_2 \left(\frac{\sin\beta_1}{L_1} - \frac{M_1}{L_1}\cos\beta_1 \kappa_0\right)}{\cos\beta_2 (M_1 \sin\beta_1 \kappa_0 + \cos\beta_1)} - \frac{\sin(\beta_2 - \gamma_2)}{L_2 \cos\beta_2}, \\ f_{\beta_1}(\beta_1, \beta_2, u) =& \frac{\cos\gamma_2 \left(\kappa_0 - \frac{\sin\beta_1}{L_1} + \frac{M_1}{L_1}\cos\beta_1 \kappa_0\right)}{\cos\beta_2 (M_1 \sin\beta_1 \kappa_0 + \cos\beta_1)}. \end{aligned} \tag{38}$$

The Jacobian linearization of the nonlinear path-following error model (34) around the origin $(\tilde{x}, \tilde{u}) = (0, 0)$ can be represented as in (21), where the matrices $A(s)$ and $B(s)$ have the following structure

$$\boldsymbol{A}(s) = \frac{\partial \tilde{\boldsymbol{f}}(s, 0, 0)}{\partial \tilde{x}} = \begin{bmatrix} 0 & 1 & 0 & 0 \\ a_{21}(s) & 0 & a_{23}(s) & 0 \\ a_{31}(s) & 0 & a_{33}(s) & a_{34}(s) \\ a_{41}(s) & 0 & a_{43}(s) & a_{44}(s) \end{bmatrix}, \tag{39}$$

and

$$\boldsymbol{B}(s) = \frac{\partial \tilde{\boldsymbol{f}}(s, 0, 0)}{\partial \tilde{u}} = \begin{bmatrix} 0 & 1 \\ 0 & b_{22}(s) \\ b_{31}(s) & b_{32}(s) \\ b_{41}(s) & b_{42}(s) \end{bmatrix}, \tag{40}$$

where

$$\begin{aligned} a_{21}(s) =& -\frac{\sin^2(\beta_{2r} - \gamma_{2r})}{L_2^2 \cos^2\beta_{2r}}, \\ a_{23}(s) =& \frac{\cos(\beta_{2r} - \gamma_{2r})}{L_2 \cos\beta_{2r}} + \frac{\sin(\beta_{2r} - \gamma_{2r}) \tan\beta_{2r}}{L_2 \cos\beta_{2r}}, \\ a_{31}(s) =& -\frac{\sin(\beta_{2r} - \gamma_{2r})}{L_2 \cos^2\beta_{2r}} \left(\frac{\cos\gamma_{2r}(\sin\beta_{1r} - \kappa_{0r} M_1 \cos\beta_{1r})}{L_1(\cos\beta_{1r} + \kappa_{0r} M_1 \sin\beta_{1r})} \right. \\ & \left. - \frac{\sin(\beta_{2r} - \gamma_{2r})}{L_2}\right), \end{aligned}$$

$$a_{33}(s) = \cos\gamma_{2r}\left(\frac{\sin\beta_{2r}(\sin\beta_{1r}-\kappa_{0r}M_1\cos\beta_{1r})}{L_1\cos\beta_{2r}^2(\cos\beta_{1r}+\kappa_{0r}M_1\sin\beta_{1r})} - \frac{1}{\cos^2\beta_{2r}L_2}\right),$$

$$a_{34}(s) = \frac{\cos\gamma_{2r}(1+\kappa_{0r}^2M_1^2)}{L_1\cos\beta_{2r}(\cos\beta_{1r}+\kappa_{0r}M_1\sin\beta_{1r})^2},$$

$$a_{41}(s) = \frac{\cos\gamma_{2r}(\kappa_{0r}L_1-\sin\beta_{1r}+M_1\cos\beta_{1r}\kappa_{0r})}{L_1L_2\cos^2\beta_{2r}(\cos\beta_{1r}+M_1\kappa_{0r}\sin\beta_{1r})}\sin(\gamma_{2r}-\beta_{2r}),$$

$$a_{43}(s) = \frac{\cos\gamma_{2r}\tan\beta_{2r}}{L_1}\left(\frac{\kappa_{0r}L_1+\kappa_{0r}M_1\cos\beta_{1r}-\sin\beta_{1r}}{\cos\beta_{2r}(\cos\beta_{1r}+\kappa_{0r}M_1\sin\beta_{1r})}\right),$$

$$a_{44}(s) = -\frac{1+\kappa_{0r}^2M_1^2+\kappa_{0r}^2L_1M_1\cos\beta_{1r}-\kappa_{0r}L_1\sin\beta_{1r}}{\sec\gamma_{2r}L_1\cos\beta_{2r}(\cos\beta_{1r}+\kappa_{0r}M_1\sin\beta_{1r})^2},$$

and

$$b_{22}(s) = -\frac{\cos(\beta_{2r}-\gamma_{2r})}{L_2\cos\beta_{2r}},$$

$$b_{31}(s) = -\frac{M_1\cos\gamma_{2r}}{L_1\cos\beta_{2r}(\cos\beta_{1r}+\kappa_{0r}M_1\sin\beta_{1r})^2},$$

$$b_{32}(s) = \frac{\cos(\beta_{2r}-\gamma_{2r})}{L_2\cos\beta_{2r}} + \frac{(\kappa_{0r}M_1\cos\beta_{1r}-\sin\beta_{1r})\sin\gamma_{2r}}{\cos\beta_{2r}L_1(\cos\beta_{1r}+\kappa_{0r}M_1\sin\beta_{1r})},$$

$$b_{41}(s) = \frac{\cos\gamma_{2r}(M_1+L_1\cos\beta_{1r})}{\cos\beta_{2r}L_1(\cos\beta_{1r}+\kappa_{0r}M_1\sin\beta_{1r})^2},$$

$$b_{42}(s) = -\frac{(\kappa_{0r}L_1+\kappa_{0r}M_1\cos\beta_{1r}-\sin\beta_{1r})\sin\gamma_{2r}}{\cos\beta_{2r}L_1(\cos\beta_{1r}+\kappa_{0r}M_1\sin\beta_{1r})}.$$

Around a straight nominal path, the system matrices in (39) and (40) simplify to

$$\boldsymbol{A} = \begin{bmatrix} 0 & 1 & 0 & 0 \\ 0 & 0 & \frac{1}{L_2} & 0 \\ 0 & 0 & -\frac{1}{L_2} & \frac{1}{L_1} \\ 0 & 0 & 0 & -\frac{1}{L_1} \end{bmatrix}, \quad \boldsymbol{B} = \begin{bmatrix} 0 & 1 \\ 0 & -\frac{1}{L_2} \\ -\frac{M_1}{L_1} & \frac{1}{L_2} \\ \frac{M_1+L_1}{L_1} & 0 \end{bmatrix}. \tag{41}$$

REFERENCES

Altafini, C. (2001). Some properties of the general n-trailer. *International Journal of Control*, 74(4), 409–424.

Altafini, C. (2003). Path following with reduced off-tracking for multibody wheeled vehicles. *IEEE Transactions on Control Systems Technology*, 11(4), 598–605.

Altafini, C. et al. (2001). A feedback control scheme for reversing a truck and trailer vehicle. *IEEE Transactions on Robotics and Automation*, 17(6), 915–922.

Bergman, K. et al. (2020). Improved path planning by tightly combining lattice-based path planning and optimal control. *Accepted for publication in IEEE Transactions on Intelligent Vehicles*. Pre-print available at arXiv: `https://arxiv.org/abs/1903.07900`.

Beyersdorfer, S. and Wagner, S. (2013). Novel model based path planning for multi-axle steered heavy load vehicles. In *Proceedings of the 16th International Conference on Intelligent Transportation Systems*, 424–429.

Evestedt, N. et al. (2016). Motion planning for a reversing general 2-trailer configuration using Closed-Loop RRT. In *Proceedings of the 2016 IEEE/RSJ International Conference on Intelligent Robots and Systems*, 3690–3697.

Faulwasser, T. et al. (2015). Nonlinear model predictive control for constrained output path following. *IEEE Transactions on Automatic Control*, 61(4), 1026–1039.

Garcia, C.E., Prett, D.M., and Morari, M. (1989). Model predictive control: theory and practice–a survey. *Automatica*, 25(3), 335–348.

Gurobi Optimization, L. (2019). Gurobi Optimizer Reference Manual. URL `http://www.gurobi.com`.

Islam, M.M. et al. (2015). A comparative study of multi-trailer articulated heavy-vehicle models. *Proceedings of the Institution of Mechanical Engineers, Part D: Journal of Automobile Engineering*, 229(9), 1200–1228.

Li, B. et al. (2019). Tractor-trailer vehicle trajectory planning in narrow environments with a progressively constrained optimal control approach. *IEEE Transactions on Intelligent Vehicles*.

Lima, P.F. et al. (2017). Spatial model predictive control for smooth and accurate steering of an autonomous truck. *IEEE Transactions on Intelligent Vehicles*, 2(4), 238–250.

Ljungqvist, O. et al. (2019). A path planning and path-following control framework for a general 2-trailer with a car-like tractor. *Journal of Field Robotics*, 36(8), 1345–1377.

Mayne, D.Q. et al. (2000). Constrained model predictive control: Stability and optimality. *Automatica*, 36(6), 789–814.

Michalek, M.M. (2014). A highly scalable path-following controller for N-trailers with off-axle hitching. *Control Engineering Practice*, 29, 61–73.

Michalek, M.M. (2019). Modular approach to compact low-speed kinematic modelling of multi-articulated urban buses for motion algorithmization purposes. In *Proceeding of the 2019 IEEE Intelligent Vehicles Symposium*, 2060–2065.

Odhams, A. et al. (2011). Active steering of a tractor–semi-trailer. *Proceedings of the Institution of Mechanical Engineers, Part D: Journal of Automobile Engineering*, 225(7), 847–869.

Orosco-Guerrero, R. et al. (2002). Modeling and dynamic feedback linearization of a multi-steered n-trailer. *IFAC Proceedings Volumes*, 35(1), 103–108.

Rimmer, A.J. and Cebon, D. (2017). Implementation of reversing control on a doubly articulated vehicle. *Journal of Dynamic Systems, Measurement, and Control*, 139(6), 061011.

Sadeghi, M.K. et al. (2019). Gain-scheduled H_∞ controller synthesis for actively steered longer and heavier commercial vehicles. *Proceedings of the Institution of Mechanical Engineers, Part D: Journal of Automobile Engineering*.

Sampei, M. and Furuta, K. (1986). On time scaling for nonlinear systems: Application to linearization. *IEEE Transactions on Automatic Control*, 31(5), 459–462.

Tilbury, D. et al. (1995). A multisteering trailer system: conversion into chained form using dynamic feedback. *IEEE Transactions on Robotics and Automation*, 11(6), 807–818.

Van De Wouw, N. et al. (2015). Active trailer steering for robotic tractor-trailer combinations. In *Proceeding of the 54th IEEE Conference on Decision and Control*, 4073–4079.

Varga, B. et al. (2018). Robust tracking controller design for active dolly steering. *Proceedings of the Institution of Mechanical Engineers, Part D: Journal of Automobile Engineering*, 232(5), 695–706.

Yuan, J., Sun, F., and Huang, Y. (2015). Trajectory generation and tracking control for double-steering tractor-trailer mobile robots with on-axle hitching. *IEEE Transactions on Industrial Electronics*, 62(12), 7665–7677.